Carbon 152 (2019) 396–408

Contents lists available at ScienceDirect

Carbon

journal homepage: www.elsevier.com/locate/carbon

Generation and characterization of carbon fiber microstructure in atomistic simulations

Kaushik Joshi [a], Mikhail I. Arefev [a, b], Leonid V. Zhigilei [a, *]

[a] Department of Materials Science and Engineering, University of Virginia, 395 McCormick Road, Charlottesville, VA, 22904-4745, USA
[b] Department of Modern Functional Materials, ITMO University, 49 Kronverksky pr., St. Petersburg, 197101, Russia

ARTICLE INFO

Article history:
Received 11 March 2019
Received in revised form
24 May 2019
Accepted 3 June 2019
Available online 4 June 2019

ABSTRACT

A clear understanding of carbon fiber (CF) microstructure is necessary for the development of high strength CFs. Here, we present an atomistic approach for generating and characterizing realistic microstructures of CFs. Large-scale reactive molecular dynamics simulations are used to generate a set of distinct CF microstructures. Comprehensive characterization of the simulated microstructures is enabled by the development of a suite of computational structural analysis tools capable of evaluation of hybridization states of carbon atoms, populations and orientations of individual carbon rings, degree of graphitization, and pore size distribution. The calculation of X-ray diffraction profiles provides a direct link between the structural features of simulated samples and experimental data available for CFs. The CF generation algorithm is shown to produce microstructures with experimental densities and with structural characteristics matching those of PAN-based CFs. The key structural features affecting the properties of CFs, such as the relative fractions of graphitic, turbostratic and amorphous microconstituents, degree of alignment, pore size distributions, and chemical cross-linking can be effectively controlled in simulations, thus enabling efficient exploration of structure–properties relationships in CFs. The capabilities of the developed approach are illustrated by performing computational analysis of the mechanical deformation and fracture of CFs under axial tensile loading.

1. Introduction

Carbon fibers (CFs) and its composites have been long pursued as an alternative to metal components because they have excellent strength to weight ratio, good thermochemical stability and high creep resistance. They are particularly attractive for automotive and aerospace applications due to their low density [1,2]. CFs can be produced using different precursors, such as polyacrylonitrile (PAN), pitch, rayon and polyethylene, with PAN precursor used in the production of a significant portion of high strength CFs [3]. The process of making CFs from precursor molecules is complex and involves several steps of chemical and thermal treatment, such as polymerization, oxidation, stabilization, carbonization and graphitization [4,5]. The exact process depends upon type of precursor and desired properties. In particular, the mechanical properties of CFs, such as Young's modulus and tensile strength, are largely controlled by the choice of the precursor molecule and fiber processing conditions, which, in turn, defines the characteristics of CF microstructure, such as crystallinity, molecular orientation, carbon content and density of defects. The fundamental understanding of the CF microstructure and its connection to the mechanical properties, however, is still lacking, which hampers the advancement of the high strength CF manufacturing techniques.

Despite some similarity of the local atomic structure of CFs to that of graphite, the microstructure of CFs is much more complex, highly sensitive to the manufacturing conditions, and hardly amenable for description in terms of a simple set of structural characteristics. It is generally believed that a CF microstructure primarily consists of layers of long sheets of sp^2-bonded carbon atoms (graphene layers). Depending on the size and arrangement of the graphene layers, they can form regions with graphitic, turbostratic or even amorphous local structural motifs. In the graphitic phase, carbon atoms exhibit sp^2 hybridization and the adjacent sheets are regularly stacked to form crystallites with a well-defined interlayer distance (d-spacing) of about 0.335 nm. The turbostratic structure is much more complex and consists of irregularly stacked carbon sheets. The d-spacing in the turbostratic carbon is higher

* Corresponding author.
E-mail address: lz2n@virginia.edu (L.V. Zhigilei).

https://doi.org/10.1016/j.carbon.2019.06.014
0008-6223/

than that in graphite, and structure may contain some atoms with sp^3 hybridization. The presence of both the graphitic and turbostratic structures in the CF microstructure has been confirmed in a number of experimental studies. For example, wide-angle X-ray scattering (WAXS) and high-resolution transmission electron microscopy (HRTEM) have been used extensively to evaluate the d-spacing and nanoscale morphology of CFs and CF-based composites [6–8]. Raman spectroscopy results show that a CF may contain sp^2, sp^3 and even amorphous carbon with predominantly sp^2 hybridization [9,10]. Another important feature of CF microstructure directly affecting the mechanical properties is the presence of defects and pores. In the existing literature, morphology of the pores in CF has been mostly studied using small-angle X-ray scattering (SAXS) measurements [11,12]. It has been reported that a typical CF microstructure has elongated pores whose lengths vary over a wide range of 30–100 nm [12,13], and their presence has negative impact on the fiber strength [14,15].

Computer simulations can further improve our understanding of complex microstructure of CFs and its correlation to the mechanical properties. Recently, atomistic simulations were applied to study the chemistry of formation of CFs. For example, molecular dynamics (MD) simulations performed with reactive force-field ReaxFF were used to investigate how cyclic rings and carbon sheets are formed from PAN [16]. ReaxFF MD was also used to study the role of physisorption and chemisorption on alignment of PAN ladders in the presence of CNT [17]. Besides the chemistry of carbonization and graphitization, MD simulations have also been used to investigate the effect of various structural defects, such as microvoids [18], specific topological defects in graphene sheets that can be generated in carbonization process [19], and faults/interfaces produced due to misorientation of graphitic domains or presence of amorphous regions [20], on the mechanical properties of CFs. While these MD simulations have provided important insights into the mechanical response of individual structural elements of CFs, the actual mechanical properties of CFs are defined by collective behavior of many structural elements comprising the complex CF microstructure and cannot be fully investigated in these simulations.

In an attempt to produce a larger-scale atomic configuration consisting of multiple graphitic domains, Ito and Okamoto [21] constructed a CF microstructure by combining 32 cuboid blocks of graphite structure into $4 \times 2 \times 4$ arrangement. The graphite crystallites had the same size but different crystallographic orientation, and were fused together to produce a regular pattern of grain boundaries by relaxing the system at 300 K in an MD simulation. A certain fraction of amorphous carbon was then introduced by randomly removing some of the carbon atoms and performing a very brief (3.6 ps) high-temperature annealing. Although this approach yielded a CF microstructure with density, graphite interlayer spacing, and Young's modulus matching the experimental values, the approach based on the regular arrangement of cuboid graphitic building blocks matching the size of crystallites in the final microstructure has its limitations and cannot be easily extended to reproduce more complex microstructure of real CFs consisting of a disordered arrangement of graphitic, turbostratic and amorphous microconstituents.

An attractive alternative to the building CF microstructure through regular arrangement of graphitic building blocks has recently been suggested by Desai et al. [22], who combined kinetic Monte Carlo (kMC) and MD methods to generate CF microstructure from small ladder-like molecules. The approach relies on structural self-organization of molecules undergoing stochastic cross-linking reactions and forming graphene sheets arranged into realistic cross-sectional microstructure (2D-microstructure) characteristic of PAN-fibers. Perfect alignment of the molecular chains along the axis of CF and the short axial length of the computational cell used in this study, however, makes it possible to only produce quasi-two-dimensional (2D) microstructures, which limits the range of applications of the model. In particular, the analysis of mechanical properties reported in Ref. [22] is limited to calculation of transverse Young's modulus, which is still affected by the perfect axial alignment of graphene sheets in the microstructure.

The objectives of the work reported in this paper are (1) to design a robust and computationally efficient method for generation of realistic three-dimensional (3D) microstructures of CFs using atomistic simulations, (2) to develop a suite of computational tools for structural characterization of the atomic configurations focused on revealing the key structural features affecting the properties of CFs and enabling direct comparison with experimental data, and (3) to demonstrate the capabilities of the developed approach by performing computational analysis of the mechanical deformation and fracture of CFs under conditions of axial tensile loading. The computational methods developed for generation and characterization of CF microstructures are described in sections 2 and 3, respectively. The computational methods are then applied for generation and structural characterization of several representative CF microstructures. Those microstructures along with their structural characteristics are discussed in section 4. The results of tensile testing simulations are reported in section 5, and the conclusions from this study are provided in section 6.

2. Computational method: generation of CF microstructure

The multi-step process of the formation of CF microstructure from molecular precursors is very complex and involves chemical reactions and structural transformations that occur on time-scales that are far beyond the capabilities of atomistic simulations. Thus, in this work we do not attempt to directly model the full chemical details of the real CF manufacturing process. Instead, we have developed a computationally-efficient alternative approach that enables generation of atomic configurations of CFs with a range of microstructures similar to those observed in experimental samples. The CF generation method is based on structural self-organization and reactive fusing of carbon ladder structural units, as described below.

2.1. Ladder structures

The idealized ladder structures used as the structural units in the computational design of CF microstructures are shown in Fig. 1. All ladders consist of three rows of hexagonal carbon rings with edges of the ladders saturated with hydrogen atoms. The choice of the ladders as the initial structural units is based on earlier studies which have reported similar intermediate structures during the manufacturing of real CFs. For example, nuclear magnetic resonance (NMR), infrared (IR) and X-ray photoelectron (XPS) spectroscopy methods were used to probe the chemical composition and structure of stabilized ladders. Those studies suggested that the stabilized PAN-fibers are primarily composed of ladder structures made of of carbon, nitrogen and hydrogen [23,24]. It is widely believed that such stabilized ladders then further undergo denitrogenation and dehydrogenation reactions to form carbon-rich sheets [4,5,25]. These sheets further re-arrange themselves to form graphitic and turbostratic phases in the CF microstructure.

To enable the generation of CFs with different microstructures and different properties, the length of the ladders was varied, and blocks of three ladders stacked into the Bernal (ABA) structural units were used as the elementary building blocks of the initial structure. The following nomenclature is used for identification of

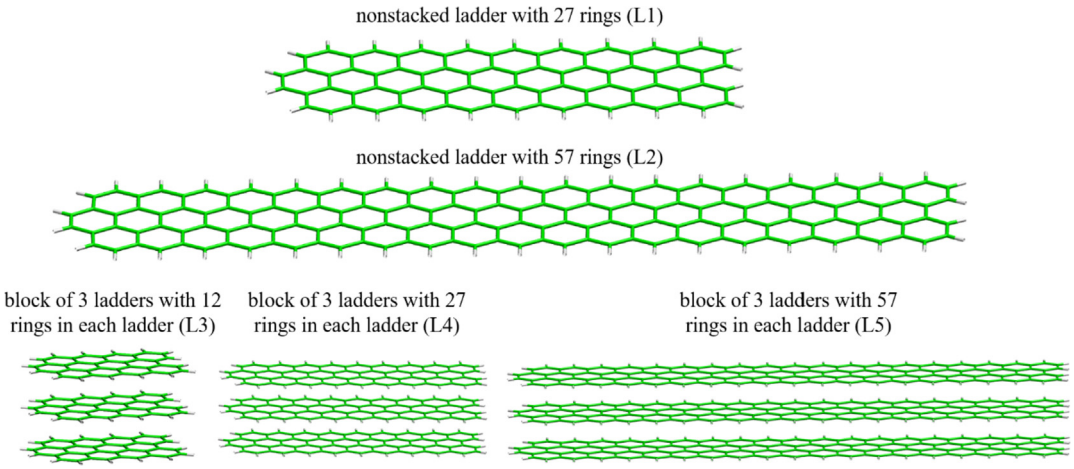

Fig. 1. The elementary building blocks used for generation of 3D microstructures of CF. Carbon atoms are shown by green color and hydrogen atoms are shown by white color. (A colour version of this figure can be viewed online.)

the ladders and the stacked three-layer blocks: The single layer ladders with lengths of 2.3 and 4.8 nm are denoted as L1 and L2, respectively, while the three-layer blocks composed of 1.1, 2.3 and 4.8 nm ladders are denoted as L3, L4 and L5, respectively. In generation of a quasi-2D CF microstructure discussed in section 4.1, a narrow ladder consisting of only two hexagonal carbon rings was used and is shown in Fig. 4a. The ladder in this case is "infinitely long" and is represented by a 2.3-nm-long segment subjected to periodic boundary condition applied in the axial direction.

2.2. Atomistic simulation procedure

The atomistic procedure used for generation of CF microstructures is schematically illustrated in Fig. 2. The ladders were initially placed in an orthogonal box using PACKMOL [26]. In addition to using different types of structural units described in section 2.1, the orientation of the units during the initial packing was varied to generate samples with different degrees of ladder alignment with respect to the CF axis. More details on the packing procedure are provided in the next section. The densities of the structures generated by PACKMOL vary between 0.6 and 1.0 g/cm^3. After applying an energy minimization procedure to the initial structures, the following steps are performed with MD method to obtain the final CF microstructures.

1. Heat the system from 1 K to 300 K in 125 ps, and then equilibrate it at 300 K for 125 ps. This step is done with a constant-temperature and constant-pressure (NPT) MD, where the pressure is maintained at 1 atm.
2. Compress the system from 1 atm to 0.3 GPa at 300 K, and then heat it from 300 K to 900 K at a constant pressure of 0.3 GPa.
3. Remove the armchair hydrogen atoms and perform NPT MD simulation at 900 K for 50 ps. During this part of MD simulation, decrease pressure in the axial direction (x-direction) from 0.3 GPa to 1 atm.
4. Remove the zigzag hydrogen atoms and perform NPT MD simulation at 900 K for 50 ps. Decrease pressure in the transverse directions (y- and z-directions) from 0.3 GPa to 1 atm. At the end of this step, entire system is at 900 K and 1 atm pressure.
5. Perform the following annealing cycle at 1 atm pressure:
   5a Heat the system from 900 K to 2000 K in 125 ps,
   5b Perform NPT MD at 2000 K for 250 ps,
   5c Cool the system from 2000 K to 300 K in 200 ps.

In graphene nanoribbons, zigzag edge is more reactive (higher bond dissociation energy) towards a hydrogen atom than armchair

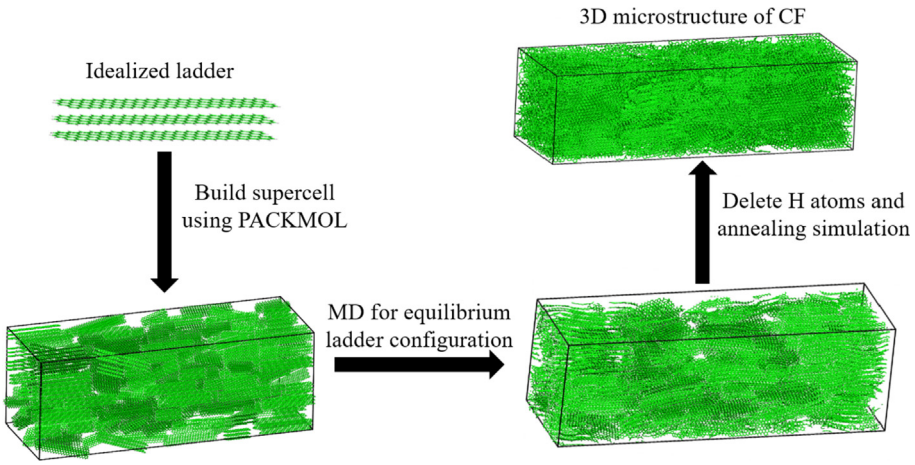

Fig. 2. Schematic of atomistic procedure for obtaining 3D microstructures of carbon fibers. Carbon atoms are shown with green color and hydrogen atoms with white color. (A colour version of this figure can be viewed online.)

edge [27]. Hence, armchair hydrogen atoms are deleted before zigzag hydrogen atoms in the CF microstructure preparation procedure. All MD simulations were performed using LAMMPS MD suite [28]. Upon deletion of hydrogen atoms (steps 3 and 4 above), unsaturated carbon atoms react with adjacent ladders thereby forming new chemical bonds. To enable the formation of new chemical bonds, MD simulations were performed using AIREBO [29], a reactive bond-order potential that has been extensively used for modeling of various carbon materials, such as carbon nanotubes [30], diamond [31], diamond nanothread [32] and carbon fibers [20]. For enhanced accuracy, a conservative timestep of 0.1 fs was used in all MD simulations except the step 1 above, where a larger timestep of 0.25 fs was used. The temperature and pressure in the NPT MD simulations were controlled with the Nosé-Hoover thermostat [33] with the effective relaxation times of temperature and pressure set to 25 fs and 2.5 ps, respectively. The three orthogonal dimensions of the periodic computational cell were allowed to change independently in the pressure control algorithm.

3. Computational method: characterization of CF microstructure

The atomic configurations produced in the simulations were then characterized by evaluation of different structural parameters, such as hybridization state of carbon atoms, cyclic rings, fiber orientation, X-ray diffraction profiles, size of the crystallites, pore size distribution, and degree of graphitization. The methods used for the calculation of these microstructure parameters are described below, and the corresponding computer codes developed in this study are available from Ref. [34].

3.1. Hybridization and ring analysis

To identify the hybridization states of carbon atoms, we calculated the number of neighbor atoms for each carbon atom. A distance cut-off of 1.7 Å was used for identifying the neighbor atoms. The carbon atoms with two, three and four neighbors were tagged as having sp, sp^2 and sp^3 hybridization, respectively.

The carbon atom ring analysis was performed using Depth-First Search (DFS) algorithm. A ring is defined as a simple loop with no cross-overs. The graph necessary for DFS is generated by building connection table of the entire system. Similar to hybridization analysis, a distance cut-off of 1.7 Å was used to build the connection table. In the graph used for the DFS search, nodes represent atoms and edges represent bonds. DFS is a recursive algorithm that uses the idea of backtracking. Starting from a node, all its adjacent nodes are pushed into a stack. Then, for moving forward, a next node is selected from the stack and its adjacent nodes are pushed into a new stack. The process is repeated until the stack is empty or the maximum ring size is reached. During the forward search, nodes that are already in the current loop are excluded. The backtracking ensures that all unvisited nodes have been traversed along the current path. A newly found ring is checked against the existing rings to ensure that each ring is identified only once. We restricted our ring search to the maximum ring size of 9.

3.2. Characterization of orientational order

The degree of orientational order in a CF microstructure can be characterized by evaluating the orientations of elemental units, such as individual ladders and graphitic carbon sheets. The realistic microstructures, however, are generally very complex due to twisting, bending and cross-linking of the elemental units. Thus, instead of identifying the orientation of the elemental units, we calculated the orientations of 5-, 6-, and 7-member carbon atom rings. The distribution of ring orientations can provide the necessary information about the degree of orientational ordering in a CF microstructure.

A ring can be described by a plane that contains the constituent atoms. In Cartesian coordinates, an equation of a plane can be written as

$$ax + by + cz = d, \tag{1}$$

where (a, b, c) corresponds to a vector normal to the plane. The ring-normal vectors were calculated using the Cartesian coordinates of ring atoms. In case of distorted or deformed rings, atoms are not perfectly coplanar. Hence, least square method was used to obtain the best fit for the ring plane. After obtaining the fit, we characterized the orientation of the ring using the following equations:

$$cos\ \alpha_x = \frac{a}{\sqrt{a^2+b^2+c^2}},\ cos\ \alpha_y = \frac{b}{\sqrt{a^2+b^2+c^2}},\ cos\ \alpha_z = \frac{c}{\sqrt{a^2+b^2+c^2}}, \tag{2}$$

where α_x, α_y and α_z are the angles the ring normal makes with x, y and z axes, respectively. Here, we assume that the x-axis is directed along the fiber axis. Hence, the normal vectors with $cos\ \alpha_x = 0$ represent the rings that are aligned along the fiber axes, *i.e.*, their normals are perpendicular to the fiber axis. Besides the ring orientation distribution, we also calculated Herman's Orientation Factor (HOF) to quantify the overall degree of orientational order in a fiber,

$$HOF = \frac{3\langle cos^2\alpha_x\rangle - 1}{2}, \tag{3}$$

where the angled brackets $\langle\ \rangle$ denote averaging over all 5-, 6-, and 7-member rings identified in the computational sample. The values of HOF can range from -0.5 to 1.0, with HOF $= 0$ corresponding to random orientation of the rings and HOF $= -0.5$ indicating that all rings are perfectly aligned along the fiber axis.

3.3. X-ray diffraction and size of crystallites

To calculate the diffraction pattern for a microstructure, we used the general procedure described in Ref. [35]. For the spherically averaged scattering profile from a system of N atoms, the scattering intensity can be written using Debye scattering equation:

$$I(Q) = \sum_{j=1}^{N}\sum_{i=1}^{N} f_i(Q) f_j(Q) \frac{\sin(Qr_{ij})}{Qr_{ij}}, \tag{4}$$

where $r_{ij} = |\vec{r_i} - \vec{r_j}|$ is a distance between atoms i and j, $Q = 4\pi \sin\theta/\lambda$ is a magnitude of a scattering vector, λ is a wavelength of an incident wave, f_i is an atomic scattering form factor of the i-th atom. If the scatterers are identical, $f_i(Q) = f_j(Q) = f(Q)$, the equation can be rewritten as

$$I(Q) = f(Q)^2\left(N + 2\sum_{j=1}^{N}\sum_{i<j}^{N}\frac{\sin(Qr_{ij})}{Qr_{ij}}\right), \tag{5}$$

Since $\frac{\sin(Qr_{ij})}{(Qr_{ij})} = \int_0^\infty \frac{\sin(Qr)}{Qr}\delta(r - r_{ij})dr$, where $\delta(r - r_{ij})$ is a delta-function, the expression (5) can be transformed to

$$I(Q) = Nf(Q)^2\left(1 + \int_0^\infty 4\pi r^2 \rho(r)\frac{\sin(Qr)}{Qr}dr\right), \quad (6)$$

where $\rho(r)$ is the pair distribution function defined as

$$\rho(r) = \frac{1}{2\pi r^2 N}\sum_{j=1}^{N}\sum_{i<j}^{N}\delta(r - r_{ij}), \quad (7)$$

The atomic scattering factor was calculated using Gaussian approximation,

$$f(\Omega)^2 = \left(\sum_{i=1}^{4} a_i \exp\left(-\frac{b_i \sin^2\theta}{\lambda^2}\right) + c\right)^2, \quad (8)$$

The coefficients in the atomic scattering factor are taken from Ref. [36]. From the diffraction pattern, we can use Scherrer equation to estimate the size of graphite crystallites along the (002) direction,

$$L_C = \frac{0.94\lambda}{B(2\theta)\cdot\cos(\theta)}, \quad (9)$$

where $B(2\theta)$ is the full width at the half maximum (FWHM) of the Gaussian approximation of the peak corresponding to d-spacing in the graphitic regions within the microstructure of CFs.

3.4. Degree of graphitization

The analysis of the degree of graphitization in CFs and carbon-carbon composites is commonly based on XRD measurements. In particular, according to the model suggested by Maire and Mering [37], the degree of graphitization can be characterized by the following parameter,

$$g_p = \frac{d_{tc} - d_{(002)}}{d_{tc} - d_{gc}}, \quad (10)$$

where d_{tc} and d_{gc} are the d-spacing in turbostratic and graphitic carbon, respectively. Defining the exact d-spacing value in turbostratic carbon, however, is not straightforward, as it can vary over a broad range from 0.344 nm to 0.367 nm [6,38,39]. Houska and Warren [40] used a structural parameter *P1* to describe the degree of graphitization. The parameter *P1* reflects the probability of adjacent hexagonal layers to have the graphitic relation and can be evaluated from XRD patterns.

In atomistic simulations, one can also use energies of carbon atoms to obtain an estimate of the degree of graphitization. The potential energies of atoms are sensitive to local structural environment, and the graphite content in a simulated microstructure can be obtained by counting the number of atoms with energies comparable to those of atoms in ideal graphite crystal. In an ideal graphite crystal at 0 K, each atom has the same energy (−7.45 eV/atom for AIREBO potential). In realistic CF microstructure, graphitic phase can be distorted and may contain defects. Hence, some tolerance to per-atom energies is necessary for accommodating energy variations due to the variability in local atomic environment. For graphite, the two most dominant local environmental factors are hybridization state of carbon atom and interlayer spacing in adjacent hexagonal layers. Since the hybridization involves chemical bonding, changes in hybridization produces significant disruption in atom energies (> 1 eV) and hence are easy to detect. However, the changes in inter-layer spacing produce relatively small variations in per-atom energies (< 100 meV) because they are primarily governed by weak van der Waals interactions. The Density Functional Theory (DFT)-based calculations have indicated that, in graphite, the interaction energy of such weak interplanar interactions varies in the range of 20–26 meV/atom [41,42]. Recently, Reguzzoni et al. used dispersion-corrected DFT (DFT-D) to calculate the interaction energy as a function of interlayer distance in bilayer graphene [43]. They reported that, in bilayer graphene, the interaction energy is approximately 30 meV/atom. Connor et al. [29] have shown that AIREBO potential agrees closely with DFT-D curve of interaction energy.

Thus, in this work, the carbon atoms of a graphitic region are identified by combining the following two criteria: (1) the carbon atom must be in sp^2 hybridization state and (2) the energy of the atom must be within 30 meV/atom from the energy of a carbon atom in an ideal graphite crystal. The degree of graphitization is then expressed as % of the carbon atoms that belong to the graphitic regions. Before evaluating the degree of graphitization, the temperature of the microstructure of interest was reduced from 300 K to 1 K in a course of an NPT MD simulation performed for 125 ps. The 1 K structure was then further energy minimized to obtain 0 K configuration.

3.5. Pore size distribution

In order to characterize the sizes and shapes of the pores present in the computational CF samples, we first identified the regions that are either empty or have very few atoms. This was done by superimposing a three dimensional grid of cubic cells on an atomistic configuration [44]. The size of each cubic cell was approximately 0.4 nm. A pore was defined as a cluster of two or more cells with less than two atoms in each cell. The cells are considered to belong to a cluster if they are connected to each other by sharing a common face or an edge. The centers of the cells in each cluster were then used to identify the pore faces, which were then used to calculate the size of the pore. The pore size was defined as a line that connects the farthest surfaces of the pore without ever crossing the pore boundary (Fig. 3). Such line vector was identified using a modified version of Bresenham's line algorithm. In this algorithm, starting from one of the points that define the pore surface, line vectors were drawn to all other points on the surface of the pore (all points are located at the centers of cell faces that outline the pore). If a vector crosses the void boundary, then it is discarded (Fig. 3). The search was performed for all pairs of surface points, and the magnitude of longest vector connecting a pair of points was taken as the pore size.

4. Microstructure of computational CFs

4.1. Microstructure of quasi-2D CFs

Before presenting the results of large-scale simulations of realistic 3D CF structures composed of graphitic, turbostratic and amorphous regions, we briefly discuss an additional simulation demonstrating that the methodology used in this study can reproduce quasi-2D cross-sectional microstructures similar to those reported in a previous atomistic study [22]. The idealized ladder used for generation of the quasi-2D microstructure is shown in Fig. 4a. It consists of 2 columns of nine 6-member rings of carbon atoms. It is 2.3-nm-long and is periodic in the *x*-direction. The computational system with lateral dimensions of 10 nm by 10 nm was filled by 200 ladders placed within the system. The total number of carbon atoms in the computational system is 15,600. To ensure periodicity, ladders were aligned along *x*-direction ($\pm 5^0$) during the initial placement, and the size of the box in this direction was set to 2.4 nm. The density of the starting configuration shown

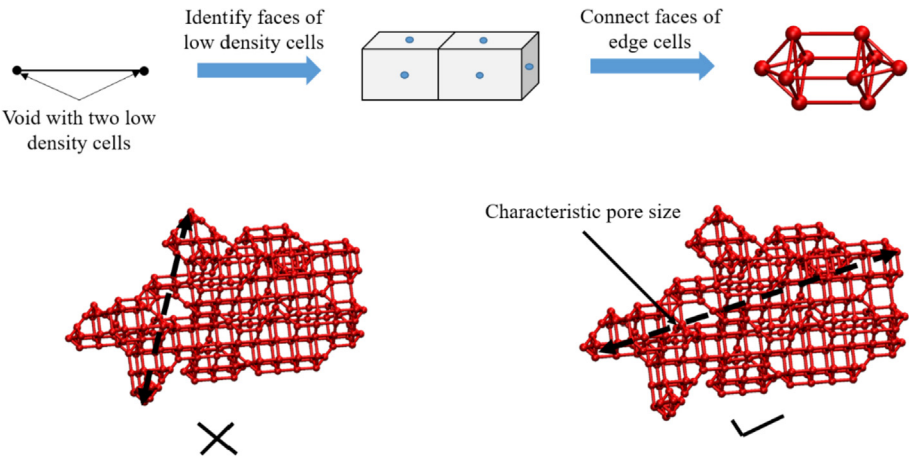

Fig. 3. Schematic representation of the method used for identification of pores and characterization of their sizes in computational CF samples. (A colour version of this figure can be viewed online.)

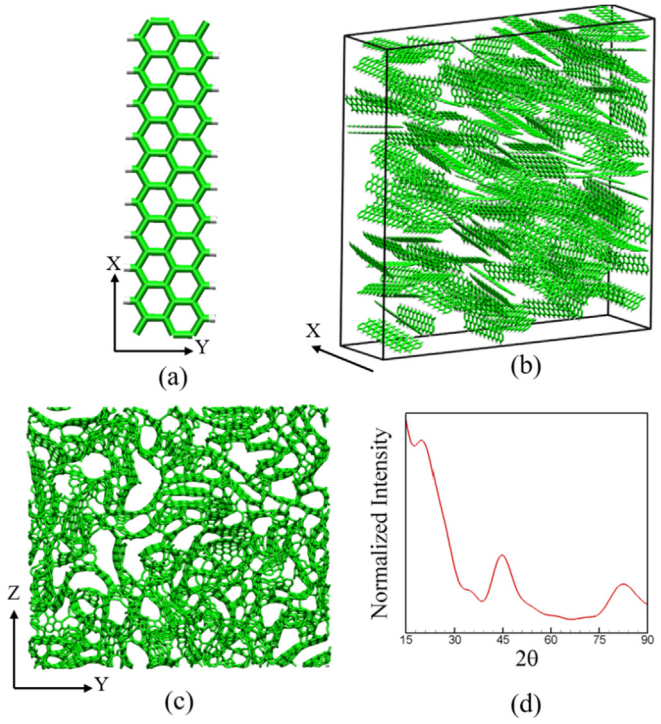

Fig. 4. The generation and characterization of a quasi-2D microstructure of a CF: (a) a single hydrogenated ladder (periodic in *x*-direction) used as an elementary unit in building the initial structure, (b) an initial configuration with ladders aligned along the *x*-axis, (c) cross-sectional (*y, z*)-view of the final quasi-2D microstructure produced at the end of the computational procedure, (d) XRD profile of the 2D microstructure. (A colour version of this figure can be viewed online.)

in Fig. 4b is 0.98 g/cm^3. The sample preparation procedure used for generation of the quasi-2D microstructure is the same as that described for 3D microstructures in section 2.2.

The *y-z* view of final microstructure is shown in Fig. 4c. Similar to computational structures generated in kMC-MD simulations [22] and observed in HRTEM images of CF cross-sections [6], the simulated microstructure exhibits curled hexagonal sheets, hairpins and pores of different sizes. We found that the structure shrinks considerably during the atomistic simulation leading to the final density of 1.79 g/cm^3, which is within the experimental range of 1.72–1.93 g/cm^3 [6,13]. The XRD profile calculated for the 2D microstructure, Fig. 4d, features two peaks near 45^0 and 78^0. These two peaks corresponds to (100) and (110) planes in graphite crystal structure, respectively, and were also found in XRD profiles calculated for CF cross-sections generated in kMC-MD simulations [22] and obtained in experimental measurements performed for CFs [6,39].

The results of this simulation suggest that the computational methodology described in section 2 and based on direct MD simulation of structural self-organization and reactive stabilization of carbon ladder structures is capable of capturing the essential features of the cross-sectional structure of CF. The quasi-2D nature of the model system, however, imposes severe limitations on the range of material properties that can be investigated in the simulations. In particular, the mechanical properties of quasi-2D CFs under conditions of axial loading are largely controlled by direct stretching of graphene layers perfectly oriented along the axis of CF, with limited contribution of the interlayer interactions and limited structural sensitivity of the mechanical properties. In order to enable realistic modeling of the mechanical properties of CFs, in the next section we apply the developed computational approach to the generation of full-3D structures produced in systems with axial size that is significantly larger than the length of the elementary structural units introduced at the initial step of the computational procedure.

4.2. Microstructure of 3D CFs

4.2.1. Initial configurations

To generate 3D microstructures with different characteristics, we used different combinations of elementary building blocks shown in Fig. 1 to create the initial configurations. To investigate the effect of alignment of ladders on fiber microstructure, we introduced a variability in the orientation of the ladders and ladder blocks while building the initial systems. The composition and alignment constraints used for building initial configurations are summarized in Table 1. For all 3D microstructures, the *x*-axis represents the fiber axis. In Fig. 5, the left-hand side panels show the snapshots of initial structures and the distributions of ladder orientations with respect to *x*- and *y*-axes. In addition to orientation constraints shown in Table 1, the ladders were initially packed with a target density of 1 g/cm^3. However, the orientation and density targets could not be fully satisfied for every system. Hence, in systems where the target constraints could not be reached with PACKMOL packing, some leeway in the initial constrains was

Table 1
Nomenclature of the initial systems used in the generation of CFs, the orientation constraints used in the generation of the systems, the corresponding HOF values, and densities after the equilibration of the systems at 1 atm and 300 K (after step 1 of the CF preparation procedure described in section 2.2). The HOF values were calculated before the equilibration at 300 K. The nomenclature refers to the elementary building blocks used in the generation of the initial systems and shown in Fig. 1, as well as to the degree of alignment of these building blocks with respect to the x-, y- and z-axes, as explained in the text.

Nomenclature	Number of atoms	Orientation constraints	HOF	Density (g/cm^3)
L1_L2_na	103,000	no constrains	0.005	1.38
L1_L2_xa	103,000	aligned ($\pm10^0$) along *x*-axis	−0.45	1.39
L3_L4_L5_xa	118,800	aligned ($\pm10^0$) along *x*-axis	−0.44	1.29
L4_L5_xa	115,200	aligned ($\pm10^0$) along *x*-axis	−0.46	1.32
L4_L5_xyza	115,200	aligned ($\pm4^0$) along *x*-, *y*- and *z*-axes	−0.49	1.39

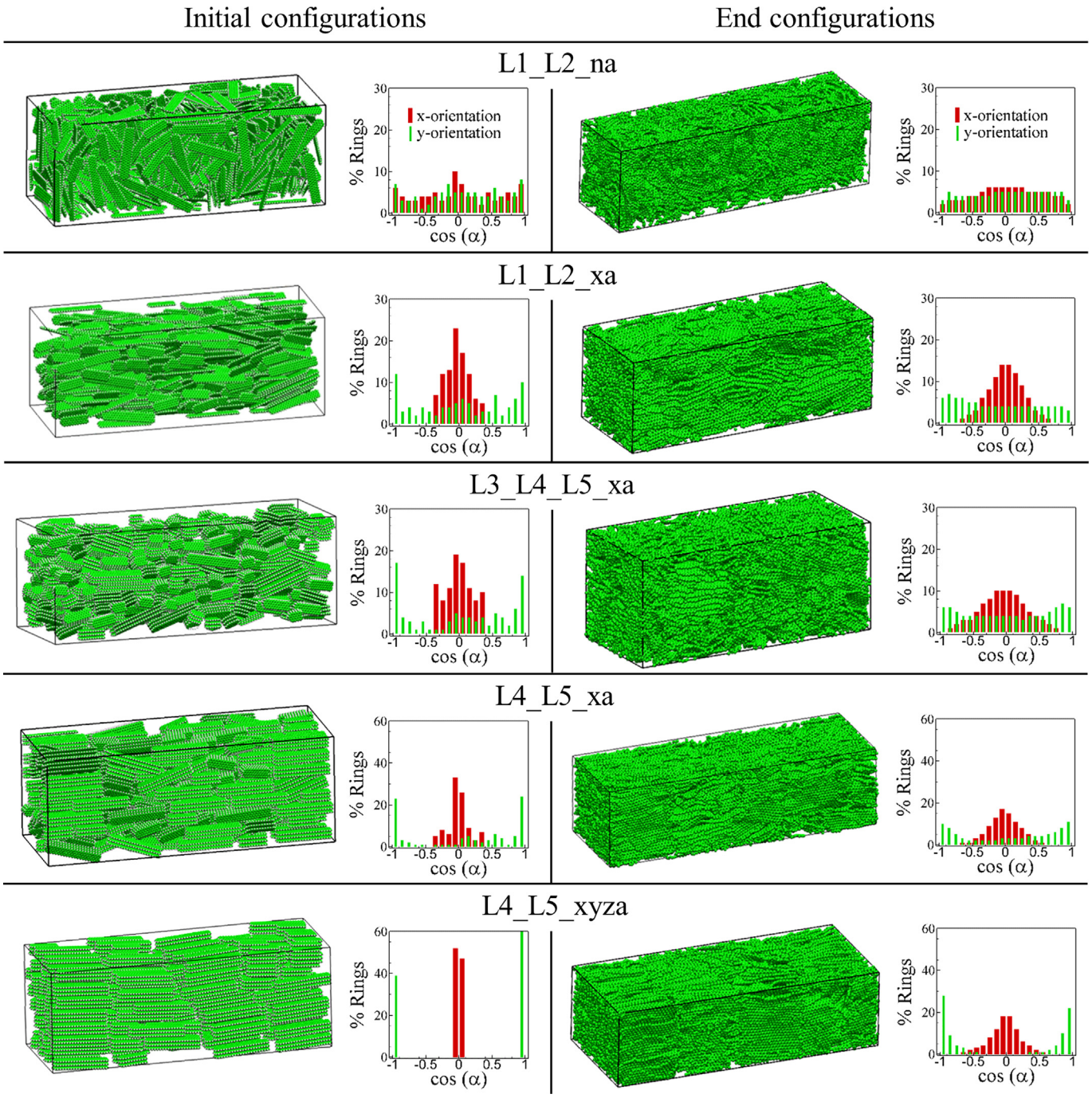

Fig. 5. Initial and final configurations of CF microstructures and corresponding distributions of the orientations of carbon ring normals with respect to the *x*- and *y*-axes. In the snapshots, carbon and hydrogen atoms are shown using green and white spheres, respectively. The distributions of orientations are calculated for 5-, 6-, and 7-member rings of carbon atoms. Data files defining the final microstructures shown in this figure are accessible from Ref. [34]. (A colour version of this figure can be viewed online.)

allowed to ensure that the density of the initial structure does not fall below 0.6 g/cm^3. For structures that are composed of two types of the elementary building blocks, each block represents 50% of the structure by weight. For structures composed of three types of blocks, each block represents approximately 33% of the structure by weight.

The first two structures listed in Table 1 and illustrated in Fig. 5 were built using non-stacked ladders L1 and L2 (see Fig. 1). The first structure (L1_L2_na) does not have any orientation constraints, which is denoted by "na," *i.e.*, non-aligned, in its nomenclature. As a result of the random orientation of ladders, this structure is characterized by a near-zero HOF value and broad orientation distributions in both *x*- and *y*-directions. In the second structure (L1_L2_xa), the ladders are preferentially aligned along the fiber axis, which is denoted by "xa" in its nomenclature. No orientation constraints were used for rotation of the ladders about the fiber axis. Hence, the orientation distribution is broad in *y*-direction and narrow in *x*-direction, where a pronounced peak around $cos\ \alpha_x = 0$ is observed. The last three structures are built from blocks of stacked ladders which are preferentially aligned along fiber axis. The structures L3_L4_L5_xa and L4_L5_xa were obtained without any orientation constraints in the (*y*, *z*)-plane. The structure L4_L5_xyza was obtained by enforcing the 3D orientation of all ladders to be within 4^0 with respect to all three axes. Hence, the orientation distributions for this system show sharp peaks at $cos\ \alpha_x = 0$ and $cos\ \alpha_y = \pm 1$. The last column in Table 1 shows that the initial alignment does not have a significant influence on material density after the equilibration of the systems at 1 atm and 300 K, *i.e.*, after step 1 of the CF preparation procedure described in section 2.2.

4.2.2. Densification and hybridization state of carbon

Starting from the initial structures generated as described in the previous section, the final CF microstructures are produced by following the processing steps outlined in section 2.2. The temporal evolution of the system density, hybridization of carbon atoms and the carbon ring population during these processing steps is exemplified for structure L4_L5_xa in Fig. 6. Other structures undergo changes similar to those shown in Fig. 6.

The deletion of the armchair and zigzag hydrogen atoms from the ladder structural elements is manifested in instantaneous drops in density of the system at 0 and 50 ps. The density, however, quickly recovers and increases rapidly due to the reactions involving sp carbon atoms appearing in the system as a result of the hydrogen removal. The reactive sp carbon atoms link with surrounding ladders to form larger carbon sheets. This linking of adjacent ladders is characterized by the sharp increase in density, population of sp^2 carbon and population of 6-member rings. It can be seen from Fig. 6 that most of the new sp^2 carbon and 6-member carbon rings are formed before the thermal annealing, and can be attributed to rapid reactions involving sp carbon atoms formed by the deletion of hydrogen.

The heating stage of the annealing cycle (step 5a in section 2.2) is characterized by a moderate density decrease due to the thermal expansion. This trend, however, is soon reversed and the fiber shrinks by ~28% during the high-temperature annealing and cool-down phases of the annealing cycle. The hybridization profiles indicate that most of the sp^3 carbon atoms are formed in the course of the heating and thermal annealing of the system. The formation of sp^3 atoms usually involves reactive sp sites creating cross-links to adjacent sheets during the shrinkage of the fiber microstructure. Out of all carbon rings identified in the final microstructure, approximately 15% are non-6-member rings, with larger rings (more than 6 members) being more numerous than the smaller 5-member rings. Note that most of the non-6-member rings are located in disordered interfacial regions separating the graphitic and turbostratic domains in the CF microstructure (see section 4.2.3 below), and do not correspond to Stone - Wales defects in the graphene sheets.

The snapshots of the final atomic configurations of CFs shown in the right-hand side panels of Fig. 5 show visually compact and largely homogeneous microstructures (pore size distributions are discussed in section 4.2.4 below). The snapshots of L1_L2_xa, L4_L5_xa, and L4_L5_xyza display more ordering and alignment of carbon sheets as compared to the other two structures. For all systems, the orientation distributions of the end structures are broader than the initial ones, which reflects bending, twisting, and reorientation of the elemental ladders in the process of linking with each other.

The information on the density, hybridization states, the number of 6-member rings, and the value of HOF characterizing the degree of alignment of graphene sheets with respect to the axis of the carbon fiber are summarized for different microstructures in Table 2. The structure L1_L2_na, with random initial orientation of ladders and HOF of the final structure closest to zero, has the lowest density, whereas the structure L4_L5_xyza with the maximum degree of the initial alignment of the ladders has the highest density. The values of density obtained for structures with ladders aligned along the fiber axis are within the experimental range of 1.72–1.96 g/cm^3 typical for CFs [6,13]. Besides the ladder alignment, the density also correlates with the fraction of sp^2 carbon. The microstructures with lower densities have lower fraction of sp^2 carbon and vice versa. The microstructures L1_L2_xa and L4_L5_xa have very similar hybridization states, HOF values, as well as nearly identical densities. The structure L4_L5_xyza has the highest fraction of sp^2 carbon, a high HOF value, and the highest density among the five samples. All these observations suggest a close connection between the hybridization state, the degree of alignment of graphene layers, and the density of fiber microstructure.

4.2.3. Diffraction profiles and degree of graphitization

As discussed in section 3.4, the degree of graphitization in the computational CF structures can be quantified through analysis of the sizes and shapes of regions with reduced potential energy in the atomic configurations, as well as by considering characteristic features of XRD profiles. The latter approach has an additional benefit of providing a direct connection to the experimental characterization of CFs [6,39].

The XRD profiles calculated for all five microstructures are shown in Fig. 7. The first peak near $2\theta = 25^0$ corresponds to the interlayer spacing (d_{002}) in graphite and can be attributed to the presence of graphitic domains of the microstructure. Previous WAXs measurements performed for CFs have reported similar d_{002} peak in the vicinity of $2\theta = 25^0$ [6,39]. The XRD signatures of graphitic domains can be correlated with the results of visual analysis of atomic configurations shown in Fig. 8, where the low-energy graphitic regions are colored blue. One can see that L1_L2_na and L3_L4_L5_xa samples contain very small regions of carbon atoms with graphite-like local structural environment scattered throughout the microstructure. As a result, these computational samples do not show any discernible d_{002} peaks in the corresponding XRD patterns. The other three microstructures show XRD peaks of different intensities and different widths indicating the presence of graphitic domains in the fiber microstructures. The values of d-spacings and characteristic sizes of graphite crystallites L_c, as calculated from XRD peaks using Eq. (8), are listed in Table 3. As explained in section 3.3, the calculation of L_c involves approximation of XRD peaks by Gaussian function. For the L1_L2_xa microstructure, however, the d_{002} peak is very broad and cannot be approximated by the Gaussian shape. Hence, the data for

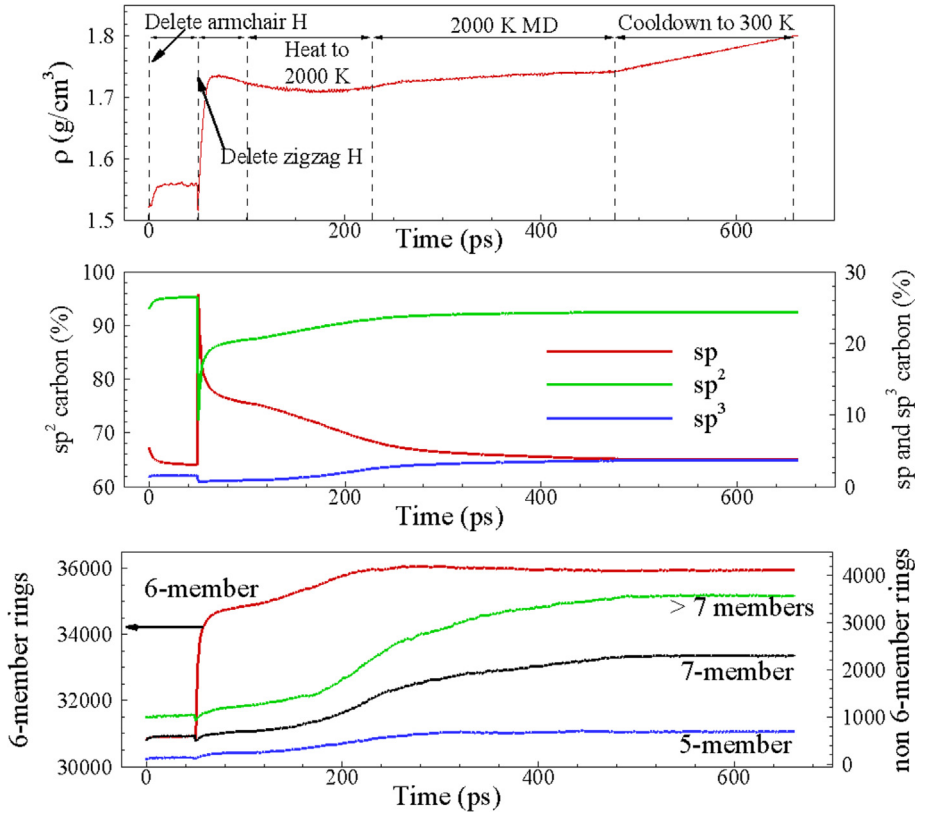

Fig. 6. Temporal evolution of fiber density, hybridization state of carbon atoms, and number of carbon rings during an MD simulation of the CF preparation procedure for structure L4_L5_xa. Similar trends have been observed for the other structures. The results are shown starting from a moment just after deletion of armchair hydrogen atoms followed by a brief local energy minimization, defined as zero time in the plots. (A colour version of this figure can be viewed online.)

Table 2
Density, dimensions of the computational cell, hybridization states, fraction of 6-member rings, and HOF of the final CF microstructures generated in MD simulations.

Structure	Density (g/cm^3)	Cell dimensions (nm × nm × nm)	sp (%)	sp^2 (%)	sp^3 (%)	6-member rings (%)	HOF
L1_L2_na	1.64	21.9 × 6.9 × 6.3	6	90.6	3.4	82.4	−0.12
L1_L2_xa	1.82	18.3 × 6.5 × 7.1	3.7	92.7	3.6	86.0	−0.37
L3_L4_L5_xa	1.72	17.4 × 7.5 × 7.7	5.8	90.9	3.3	80.0	−0.29
L4_L5_xa	1.80	21.6 × 7.4 × 6.1	3.8	92.5	3.7	84.6	−0.389
L4_L5_xyza	1.93	19.5 × 8.4 × 5.6	2.2	95	2.8	87.7	−0.385

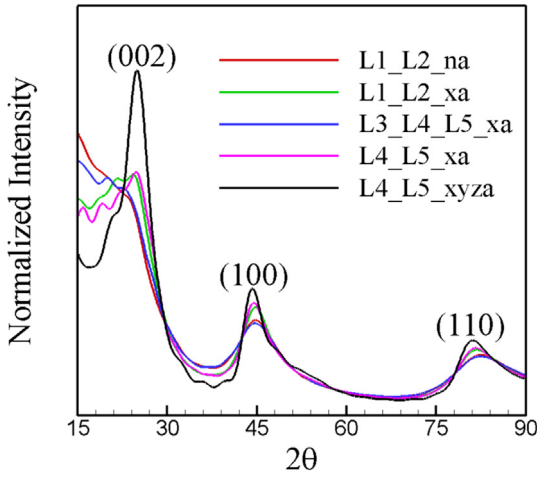

Fig. 7. XRD profiles calculated for five computational CF samples. (A colour version of this figure can be viewed online.)

this structure is not included in Table 3. The presence of such a broad peak indicates that L1_L2_xa has small graphite regions (≤3 layers) that are dispersed in the microstructure. This assertion is supported by the visual analysis of the corresponding atomic configuration in Fig. 8.

The remaining two microstructures have sharper XRD peaks indicating the presence of sizeable graphite crystallites (>3 layers). The sizeable graphite crystallites in these two microstructures are clearly visible in Fig. 8. Among the five microstructures, the largest graphite crystallites are found in L4_L5_xyza microstructure, which also exhibits the sharpest XRD peak corresponding to the d-spacing. The microstructure of the L4_L5_xyza sample is further illustrated by thin slices cut in transverse and longitudinal directions and shown in Fig. 9. One can see from this figure that the graphitic regions composed of layered carbon sheets are separated from each other by non-graphitic regions containing curled sheets, cross-links, hairpins and amorphous carbon. The experimental studies [6,13] have reported that for pitch-based fibers the d-spacing varies in the range of 0.338–0.344 nm, and the graphite crystallite size varies in the range of 2–25 nm. The corresponding values for PAN-based fibers are from 0.342 to 0.351 nm and from 1.5

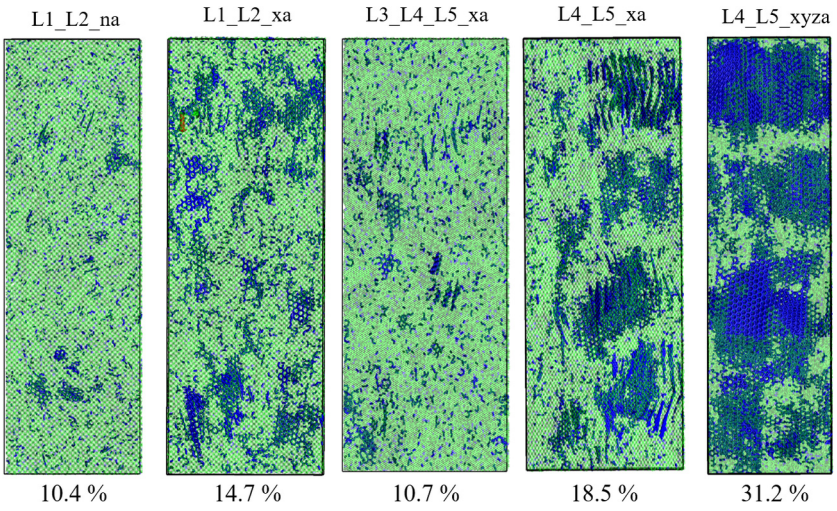

Fig. 8. Snapshots of 3D CF microstructures showing graphitic regions. The carbon atoms that belong to graphitic regions have lower potential energies and are shown in blue color, while the remaining carbon atoms are shown in semi-transparent green color. The numbers at the bottom show the degree of graphitization of the corresponding microstructures. Data files defining the CF microstructures shown in this figure are accessible from Ref. [34]. (A colour version of this figure can be viewed online.)

Table 3
d_{002} spacing and size of graphitic domains as estimated from XRD profiles.

Structure	2θ	d_{002} spacing (nm)	Crystallite size, L_c (nm)
L4_L5_xa	25.064	0.355	1.49
L4_L5_xyza	24.99	0.356	2.11

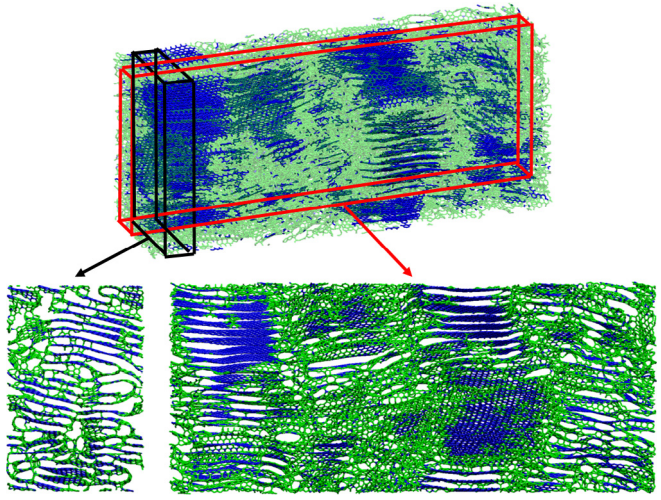

Fig. 9. Close-up views of cross-sections (2-nm-thin slices) of L4_L5_xyza microstructure showing graphitic, turbostratic and amorphous carbon phases. The location of the transverse and longitudinal sections are shown by black and red rectangular boxes, respectively. Graphitic atoms are colored blue and remaining atoms are colored green. (A colour version of this figure can be viewed online.)

to 7.8 nm, respectively. Hence, the graphitic phases observed in the simulated microstructures have characteristics similar to those in the PAN-based fibers. It should be noted that the lateral dimensions of the computational system (~5–8 nm, see Table 2) put a natural limit on the maximum size of the graphitic crystallites that can be generated in the sample preparation process. Larger crystallites can be formed with the approach developed in this work if simulations are performed for larger computational systems.

The other two peaks in the diffraction profiles shown in Fig. 7, near 45^0 and 80^0, corresponds to (100) and (110) planes in the graphite crystal structure, respectively. The (100) and (110) peaks have also been observed in experimental measurements [6,39]. Unlike d_{002} peak, these two peaks are visible in all five microstructures, since they arise from the atomic ordering within the graphene planes present in all computational CF structures.

4.2.4. Shapes and sizes of pores

An important factor that controls the properties of CFs is the presence of pores and their size distribution. The shapes of the maximum pores present in the computer-generated CF structures and the volume fractions of pores of different sizes are shown in Fig. 10, while the 2D views (projections to XY plane) of all pores are provided for each microstructure in Fig. 11. For all computational samples, the smaller pores with characteristic sizes between 1 and 2 nm contribute the most to the total porosity of the material. The microstructures with lower densities exhibit narrower size distributions with larger volume fractions of small pores. The pore size distribution tends to gets broader with the increase in density. The largest pore with a characteristic size of about 8 nm is found in L4_L5_xa sample.

Fig. 11 shows that most of the pores observed in the simulated microstructures have elongated shapes. The smaller pores have shapes of elongated ellipsoids. However, the elongated shapes become more irregular with the increase in pore size. The majority of the elongated pores are aligned along the fiber axis (Fig. 11) and are mostly located at the boundaries between misoriented crystallites. A small-angle x-ray scattering (SAXS) experimental study aimed at identification of microvoids in PAN-based CFs has also revealed the presence of aligned and elongated pores [12]. The pores identified in the PAN-based fibers have elongated shapes with width/dimeter in the range of 0.5–3.0 nm and length in the range of 30–100 nm. Given the total length of the computational systems of about 20 nm (see Table 2), we cannot expect to match the experimentally observed pore length values in the simulated samples. Nevertheless, the shapes and sizes of the voids are in a reasonable semi-quantitative agreement with the experimental observations.

5. Mechanical properties

The development of a robust and nimble method for the generation of realistic models of CFs, combined with a set of

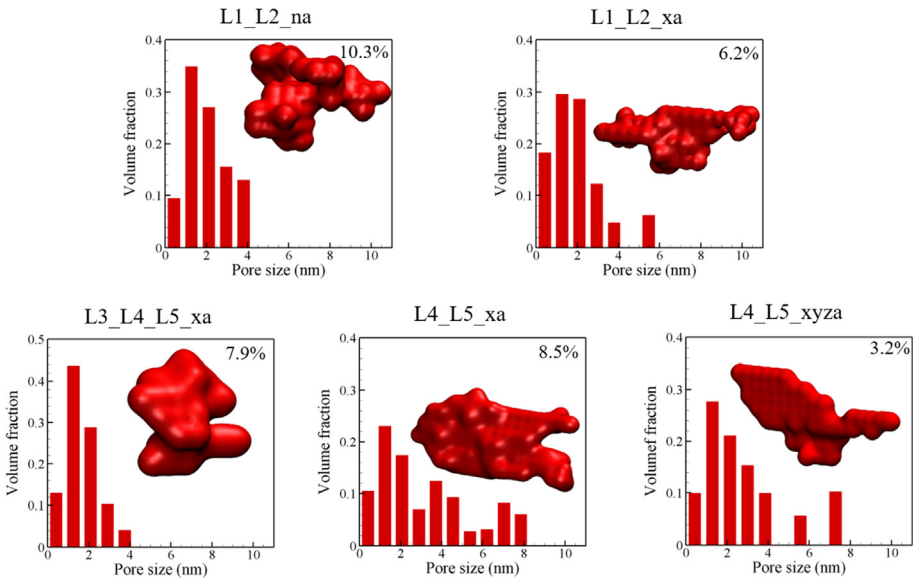

Fig. 10. Pore size distributions and shapes of the largest voids found in each of the five 3D CF microstructures generated in the atomistic simulations. For obtaining the size distributions, pores were binned based on their size. The bin width was set to 0.8 nm. The porosity (volume fraction of all pores) is listed on each panel in units of volume percent. (A colour version of this figure can be viewed online.)

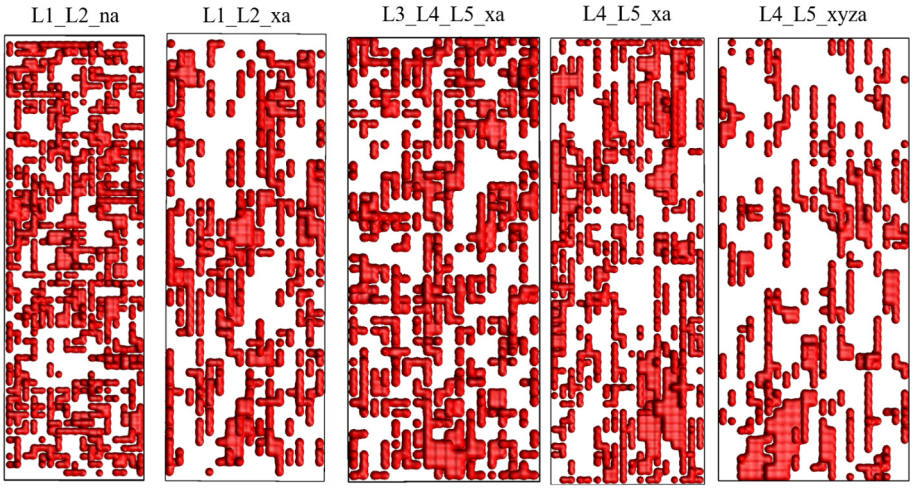

Fig. 11. 2D view (XY-view) of all pores in computer generated microstructures. Pores are shown by red color. The carbon atoms surrounding the voids are not shown for better visualization. (A colour version of this figure can be viewed online.)

computational tools for characterization of CF microstructure, provide a broad range of opportunities for investigation of mechanical and thermal transport properties of CFs. In this section, we illustrate these opportunities by briefly describing first results of atomistic simulations aimed at investigation of the mechanical behavior of CFs under condition of axial tensile loading. The simulations are performed for the five computational samples described in the previous sections. Each of the samples was stretched along the fiber axis (x-direction) at a strain rate of 2.5×10^8 sec^{-1}. A constant pressure of 1 atm was maintained in the lateral (y and z) directions. The tensile testing simulations were performed using AIREBO potential. Previous studies have shown that AIREBO potential exhibit non-physical strain hardening at high tensile stresses due to the use of a switching function applied within a narrow range of interatomic distances and enforcing dissociation of chemical bonds by 2.0 Å [32,45,46]. In order to alleviate this shortcoming, the inner cut-off distance for the onset of the application of the switching function was extended to 2 Å, as suggested in Ref. [31]. The stress-strain curves and the corresponding mechanical properties of different microstructures are shown in Fig. 12 and listed Table 4, respectively. One can see that the mechanical properties can be correlated to both the degree of alignment of graphene sheets along the axis of the carbon fiber and the extent of graphitization. The values of Young's modulus of the two structures with scant presence of graphitic phase (L1_L2_na and L3_L4_L5_xa) are about 60 and 40% lower than the remaining three structures. The moduli of the three structures with more substantial presence of graphitic phase are within the range of experimental values of 231–510 GPa reported for PAN-based fibers [6,13]. The comparison of systems with comparable fractions of graphitic phase also suggests that the Young's modulus increases with increased level of alignment of the structural elements along the axis of the fiber.

The shapes of the stress-strain curves shown in Fig. 12 indicate that the degree of structural alignment also affects the fracture

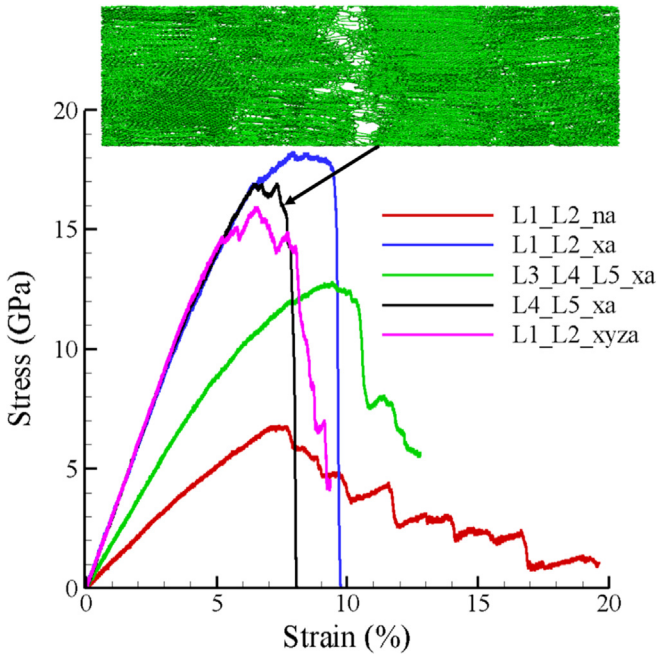

Fig. 12. Stress-strain curves predicted in simulations of axial loading of the five CF samples generated in the present work. The strain rate of 2.5×10^8 sec^{-1} was used in the simulations. (A colour version of this figure can be viewed online.)

behavior. The well-aligned structures L1_L2_xa, L4_L5_xa, and L4_L5_xyza have HOF < −0.37 and exhibit high strength and brittle failure under tensile loading. The least aligned L1_L2_na structure with HOF = −0.12 exhibits a considerably lower tensile strength and a gradual decrease of stress after the onset of failure, while the structure with an intermediate HOF = −0.29 shows an intermediate fracture behavior as well. The values of the tensile strength and tensile strain at fracture predicted in the simulations are higher than the experimental values measured for PAN-based fibers [6,13]. The overestimation of the tensile strength in atomistic simulations is an expected result related to the ultrahigh loading rate and the low limit on the maximum pore size imposed by the relatively small size of the computational cell used in the simulations.

Interestingly, for structures with significant fractions of graphitic phase, the tensile strength and tensile strain at fracture decreases with the increase in graphite content. This observation suggests that the dependence of the mechanical properties of CFs on the microstructure cannot be reduced to a dependence on a single structural parameter, such as degree of graphitization. A combined effect of various structural characteristics, including the distribution and shapes of nano-/micro-pores, relative fractions of graphitic, turbostratic, and amorphous regions, their distribution in the fiber, properties of interfaces separating the different regions, as well as the degree of structural alignment, should be considered for a complete understanding of the structural origins of the mechanical behavior of CFs. The results of the first simulations briefly discussed in this section suggest that large-scale atomistic simulations are well suited for systematic exploration of the multidimensional space of parameters defining the complex structure − mechanical properties relationships in CFs.

6. Summary

A robust and computationally efficient approach is developed for generation and structural characterization of atomistic 3D microstructures of CFs. The microstructures are generated from initial configurations built by assembling idealized hydrogenated carbon sheets or blocks of ladders of different sizes and orientations. The initial systems are then modified by applying a sequence of equilibration, compression, dehydrogenation, high-temperature annealing and relaxation steps, all performed within reactive molecular dynamics simulations.

A comprehensive characterization of the simulated microstructures is enabled by the development of a suite of computational structural analysis tools suitable for revealing the key structural features affecting the properties of CFs and establishing direct links to experimental data. In particular, the hybridization state of each carbon atom is identified by the number of nearest neighbors interacting chemically with the atom. The ring analysis is performed using the DFS algorithm. The orientational order and the degree of alignment of structural elements along the axis of the fiber are characterized through analysis of orientation of individual carbon rings and calculation of HOF averaged over the whole sample. The atomic energies are used for identification of the graphitic domains and quantification of the degree of graphitization in different microstructures. The Bresenham's line algorithm is used for identification of the pore shapes and pore size distributions. The calculation of XRD profiles makes it possible to connect the spacing between graphitic carbon sheets and the characteristic size of the crystalline domains in the simulated CF microstructures to the results of experimental measurements.

The application of the CF generation algorithm has demonstrated its ability to produce microstructures with various relative fractions of graphitic, turbostratic and amorphous microconstituents, different degrees of alignment of the structural elements with respect to the fiber axis, and different densities of chemical cross-linking between carbon sheets. The densities of the computer-generated microstructures lie within the experimental range of 1.72–1.96 g/cm^3. The characteristic sizes of graphitic domains and interlayer spacing within these domains calculated from the diffraction profiles are also found to be in a good quantitative agreement with experimental values obtained from XRD data for PAN-based fibers. The analysis of pore shapes and sizes reveals the presence of elongated pores aligned preferentially along the fiber axis. The shapes and lateral sizes of the pores in the computational samples are similar to those obtained for PAN-based CFs in SAXS experiments. Overall, the structural characteristics of computer-generated microstructures are matching those of real PAN-based CFs, suggesting that the developed computational approach is

Table 4
Degree of graphitization and mechanical properties of computational CF microstructures predicted in simulations of axial tensile loading. The corresponding stress-strain curves are shown in Fig. 12.

Structure	Degree of graphitization (%)	Young's modulus (GPa)	Tensile strength (GPa)	Tensile strain (%)
L1_L2_na	10.4	102.8	6.62	7.7
L1_L2_xa	14.7	278.7	18.2	7.9
L3_L4_L5_xa	10.7	175.6	12.7	9.4
L4_L5_xa	18.5	279.4	16.9	7.3
L4_L5_xyza	31.2	284.5	15.9	6.6

suitable for the systematic analysis of the structure – properties relationships in CFs.

As an example of applications of the developed computational methodology, a series of atomistic simulations of axial tensile loading are performed for five representative CF microstructures. The results of the simulations reveal an important role of the orientational ordering in the CF structure. The computational samples with high degree of alignment of structural elements have high values of Young's modulus that match those measured in experiments. The samples with lower degree of structural alignment exhibit softer elastic response characterized by considerably lower values of Young's modulus. In general, the first simulations revel a complex dependence of the mechanical properties of CFs on various structural characteristics and highlight the need for further systematic analysis of this dependence. The methodology presented in this work has a high promise for enabling the investigation of the structure-property relationships and fracture mechanics in atomistic simulations of CFs.

Acknowledgements

Financial support for this work was provided by the U.S. Department of Energy's Office of Energy Efficiency and Renewable Energy (EERE) under the Vehicle Technologies Office Award Number DE-EE0008195. Computational support is provided by the National Science Foundation through the Extreme Science and Engineering Discovery Environment (Project CTS160026 and MSS180008) and by the Oak Ridge Leadership Computing Facility (INCITE project MAT130).

References

[1] A. Jacob, Carbon fibre and cars – 2013 in review, Reinforced Plastics 58 (1) (2014) 18–19.
[2] F. Meng, J. McKechnie, T. Turner, K.H. Wong, S.J. Pickering, Environmental aspects of use of recycled carbon fiber composites in automotive applications, Environ. Sci. Technol. 51 (21) (2017) 12727–12736.
[3] H.G. Chae, B.A. Newcomb, P.V. Gulgunje, Y. Liu, K.K. Gupta, M.G. Kamath, K.M. Lyons, S. Ghoshal, C. Pramanik, L. Giannuzzi, K. Şahin, I. Chasiotis, S. Kumar, High strength and high modulus carbon fibers, Carbon 93 (2015) 81–87.
[4] X. Huang, Fabrication and properties of carbon fibers, Materials 2 (4) (2009) 2369–2403.
[5] E. Frank, L.M. Steudle, D. Ingildeev, J.M. Sporl, M.R. Buchmeiser, Carbon fibers: precursor systems, processing, structure, and properties, Angew. Chem. Int. Ed. 53 (21) (2014) 5262–5298.
[6] S. Kumar, D.P. Anderson, A.S. Crasto, Carbon fibre compressive strength and its dependence on structure and morphology, J. Mater. Sci. 28 (2) (1993) 423–439.
[7] J. Zhao, L. Yang, F. Li, R. Yu, C. Jin, Structural evolution in the graphitization process of activated carbon by high-pressure sintering, Carbon 47 (3) (2009) 744–751.
[8] L. Dobiášová, V. Starý, P. Glogar, V. Valvoda, Analysis of carbon fibers and carbon composites by asymmetric X-ray diffraction technique, Carbon 37 (3) (1999) 421–425.
[9] H. Okuda, R.J. Young, D. Wolverson, F. Tanaka, G. Yamamoto, T. Okabe, Investigating nanostructures in carbon fibres using Raman spectroscopy, Carbon 130 (2018) 178–184.
[10] M.A. Kim, D. Jang, S. Tejima, R. Cruz-Silva, H.I. Joh, H.C. Kim, S. Lee, M. Endo, Strengthened PAN-based carbon fibers obtained by slow heating rate carbonization, Sci. Rep. 6 (2016) 22988.
[11] D.J. Johnson, C.N. Tyson, The fine structure of graphitized fibres, J. Phys. D Appl. Phys. 2 (6) (1969) 787–795.
[12] A.F. Thünemann, W. Ruland, Microvoids in polyacrylonitrile fibers: A small-angle X-ray scattering study, Macromolecules 33 (5) (2000) 1848–1852.
[13] S. Ozcan, F. Vautard, A.K. Naskar, Designing the structure of carbon fibers for optimal mechanical properties, in: Polymer Precursor-Derived Carbon, American Chemical Society, 2014 , pp. 215–232.
[14] W. Jiang, Z. Huang, Y. Wang, B. Zheng, H. Zhou, Voids formation and their effects on mechanical properties in thermoformed carbon fiber fabric-reinforced composites , Polym. Compos. 40 (S2) (2019) E1094–E1102.
[15] C. Zhu, X. Liu, J. Guo, N. Zhao, C. Li, J. Wang, J. Liu, J. Xu, Relationship between performance and microvoids of aramid fibers revealed by two-dimensional small-angle X-ray scattering, J. Appl. Crystallogr. 46 (4) (2013) 1178–1186.
[16] B. Saha, G.C. Schatz, Carbonization in polyacrylonitrile (PAN) based carbon fibers studied by ReaxFF molecular dynamics simulations, J. Phys. Chem. B 116 (15) (2012) 4684–4692.
[17] B. Saha, A. Furmanchuk, Y. Dzenis, G.C. Schatz, Multi-step mechanism of carbonization in templated polyacrylonitrile derived fibers: ReaxFF model uncovers origins of graphite alignment, Carbon 94 (2015) 694–704.
[18] C. Zhu, X. Liu, X. Yu, N. Zhao, J. Liu, J. Xu, A small-angle X-ray scattering study and molecular dynamics simulation of microvoid evolution during the tensile deformation of carbon fibers, Carbon 50 (1) (2012) 235–243.
[19] N. Gupta, V.I. Artyukhov, E.S. Penev, B.I. Yakobson, Carbonization with mis-fusion: fundamental limits of carbon-fiber strength revisited, Adv. Mater. 28 (46) (2016) 10317–10322.
[20] E.S. Penev, V.I. Artyukhov, B.I. Yakobson, Basic structural units in carbon fibers: atomistic models and tensile behavior, Carbon 85 (2015) 72–78.
[21] A. Ito, S. Okamoto, Using molecular dynamics to assess mechanical properties of PAN-based carbon fibers comprising imperfect crystals with amorphous structures, Int. J. Mech. Aero. Indus. Mechatr. Manufac. Eng. 7 (9) (2013) 1839–1845.
[22] S. Desai, C. Li, T. Shen, A. Strachan, Molecular modeling of the microstructure evolution during carbon fiber processing, J. Chem. Phys. 147 (22) (2017) 224705.
[23] K. Morita, Y. Muruta, A. Ishitani, K. Murayama, T. Ono, A. Nakajima, Characterization of commercially available PAN (polyacrylonitri1e)-based carbon fibers, Pure Appl. Chem. 58 (3) (1986) 455–468.
[24] Z. Bashir, A critical review of the stabilisation of polyacrylonitrile, Carbon 29 (8) (1991) 1081–1090.
[25] A.K. Gupta, D.K. Paliwal, P. Bajaj, Acrylic precursors for carbon fibers, J. Macromol. Sci., Part C 31 (1) (1991) 1–89.
[26] L. Martínez, R. Andrade, E.G. Birgin, J.M. Martínez, PACKMOL: A package for building initial configurations for molecular dynamics simulations, J. Comput. Chem. 30 (13) (2009) 2157–2164.
[27] D.E. Jiang, B.G. Sumpter, S. Dai, Unique chemical reactivity of a graphene nanoribbon's zigzag edge, J. Chem. Phys. 126 (13) (2007) 134701.
[28] S. Plimpton, Fast parallel algorithms for short-range molecular dynamics, J. Comput. Phys. 117 (1) (1995) 1–19.
[29] T.C. O'Connor, J. Andzelm, M.O. Robbins, AIREBO-M: A reactive model for hydrocarbons at extreme pressures, J. Chem. Phys. 142 (2) (2015), 024903.
[30] Y.I. Jhon, C. Kim, M. Seo, W.J. Cho, S. Lee, Y.M. Jhon, Tensile characterization of single-walled carbon nanotubes with helical structural defects, Sci. Rep. 6 (2016) 20324.
[31] O.A. Shenderova, D.W. Brenner, A. Omeltchenko, X. Su, L.H. Yang, Atomistic modeling of the fracture of polycrystalline diamond, Phys. Rev. B 61 (6) (2000) 3877–3888.
[32] H. Zhan, G. Zhang, V.B. Tan, Y. Cheng, J.M. Bell, Y.W. Zhang, Y. Gu, From brittle to ductile: a structure dependent ductility of diamond nanothread, Nanoscale 8 (21) (2016) 11177–11184.
[33] W. Shinoda, M. Shiga, M. Mikami, Rapid estimation of elastic constants by molecular dynamics simulation under constant stress, Phys. Rev. B 69 (13) (2004) 134103.
[34] http://www.faculty.virginia.edu/CompMat/carbon-structure-analysis/.
[35] Z. Lin, L.V. Zhigilei, Time-resolved diffraction profiles and atomic dynamics in short-pulse laser-induced structural transformations: molecular dynamics study, Phys. Rev. B 73 (18) (2006) 184113.
[36] P.J. Brown, A.G. Fox, E.N. Maslen, M.A. O'Keefe, B.T.M. Willis, Intensity of diffracted intensities, in: International Tables for Crystallography, vol. C: Mathematical, Physical and Chemical Tables, Springer, Dordrecht, 2006, pp. 554–595.
[37] L. Zou, B. Huang, Y. Huang, Q. Huang, C. Wang, An investigation of heterogeneity of the degree of graphitization in carbon–carbon composites, Mater. Chem. Phys. 82 (3) (2003) 654–662.
[38] M.A. Short, P.L. Walker, Measurement of interlayer spacings and crystal sizes in turbostratic carbons, Carbon 1 (1) (1963) 3–9.
[39] D.P. Anderson, Carbon Fiber Morphology, II: Expanded Wide-Angle X-Ray Diffraction Studies of Carbon Fibers, University of Dayton Research Institute, 1991.
[40] C.R. Houska, B.E. Warren, X-Ray study of the graphitization of carbon black, J. Appl. Phys. 25 (12) (1954) 1503–1509.
[41] M.C. Schabel, J.L. Martins, Energetics of interplanar binding in graphite, Phys. Rev. B 46 (11) (1992) 7185–7188.
[42] J.C. Charlier, X. Gonze, J.P. Michenaud, Graphite interplanar bonding: electronic delocalization and van der Waals interaction, Europhys. Lett. (EPL) 28 (6) (1994) 403–408.
[43] M. Reguzzoni, A. Fasolino, E. Molinari, M.C. Righi, Potential energy surface for graphene on graphene: Ab initioderivation, analytical description, and microscopic interpretation, Phys. Rev. B 86 (24) (2012) 245434.
[44] E. Leveugle, D.S. Ivanov, L.V. Zhigilei, Photomechanical spallation of molecular and metal targets: molecular dynamics study, Appl. Phys. A 79 (7) (2004) 1643–1655.
[45] H. Zhao, K. Min, N.R. Aluru, Size and chirality dependent elastic properties of graphene nanoribbons under uniaxial tension, Nano Lett. 9 (8) (2009) 3012–3015.
[46] C. Carpenter, D. Maroudas, A. Ramasubramaniam, Mechanical properties of irradiated single-layer graphene, Appl. Phys. Lett. 103 (1) (2013) 013102.